Applied Catalysis B: Environmental 199 (2016) 187–198

Contents lists available at ScienceDirect

Applied Catalysis B: Environmental

journal homepage: www.elsevier.com/locate/apcatb

ZnO quantum dots decorated 3DOM TiO_2 nanocomposites: Symbiose of quantum size effects and photonic structure for highly enhanced photocatalytic degradation of organic pollutants

Meryam Zalfani[a,b], Benoit van der Schueren[a], Mounira Mahdouani[b], Ramzi Bourguiga[b], Wen-Bei Yu[c], Min Wu[c,**], Olivier Deparis[d], Yu Li[c,**], Bao-Lian Su[a,c,e,*]

[a] Laboratory of Inorganic Materials Chemistry (CMI), University of Namur, 61 rue de Bruxelles, B-5000 Namur, Belgium
[b] Laboratoire de Physique des Matériaux: Structure et Propriétés, Groupe Physique des Composants et Dispositifs Nanométriques, Faculté des Sciences de Bizerte, University of Carthage, 7021 Jarzouna-Bizerte, Tunisia
[c] State Key Laboratory of Advanced Technology for Materials Synthesis and Processing, Wuhan University of Technology, Luoshi Road 122, 430070, Wuhan, Hubei, China
[d] Departement of Physics, University of Namur, Rue de Bruxelles 61, B-5000 Namur, Belgium
[e] Clare Hall, University of Cambridge, Cambridge, United Kingdom

ARTICLE INFO

Article history:
Received 18 March 2016
Received in revised form 1 June 2016
Accepted 4 June 2016
Available online 23 June 2016

Keywords:
ZnO quantum dots
3DOM TiO_2
Quantum size effect
Light sensitizor
Photonic effect

ABSTRACT

Three dimensionally ordered macroporous inverse opal TiO_2 nanocomposites decorated by ZnO quantum dots (ZnO QDs@3DOM TiO_2) with an intimate contact were successfully synthesized using the sol-gel technique and characterized in terms of structure, porosity, chemical composition and optical properties. The photocatalytic activity of ZnO QDs@3DOM TiO_2 nanocomposites with different ZnO QDs amounts was evaluated in the aqueous phase of dye pollutant molecules and compared with the state-of-the-art 3DOM TiO_2 and P25 photocatalysts. The symbiotic effect of ZnO QDs and 3DOM photonic structure on the light absorption and further on the photocatalytic activity of the nanocomposites was observed. The sample with the highest ZnO QDs amount exhibits extraordinarily high photocatalytic activity, which is attributed to firstly, the formation of an intimate junction between the two semiconductors, hence favoring the separation of photo-introduced electron–hole pairs in ZnO-TiO_2 photocatalyst, and, secondly, to the quantum size effect (QSE). The QSE results in an increase in the width of the forbidden electronic band, which increases the energy of electrons (holes) in the conduction (valence) and particularly leads to the displacement of the conduction band potentials of ZnO to more negative energy values compared to TiO_2. Thanks to the heterojuction formed between ZnO QDs and 3DOM TiO_2, the energy difference between conduction bands of both semiconductors acts as a driving force for rapid electron/hole transfer between the coupled materials. Due to the extremely short diffusion time, the lifetime of photogenerated charge carriers is extended and the effectiveness of reduction and oxidation process is increased with faster reaction kinetics. Increasing the amount of ZnO QDs can boost the photocatalytic activity. On the other hand, 3DOM photonic structure of TiO_2 with its open meso-macroporosity can facilite the diffusion of dye molecules and light propagation. This first successful example of symbiose of a series of physical effects can open a new window for solar energy conversion by the synergitic association of QSEs, photonic effect and other effects such as plasmonic effects, in one solid material to develop highly efficient solar light havesting system to enhance solar energy conversion effeciency for photocatalysis and photovoltaics.

1. Introduction

Photocatalytic degradation of organic pollutants and water splitting process using semiconductors such as TiO_2 and ZnO have been extensively investigated in order to solve environmental and energy problems [1–3]. ZnO is a direct band gap semiconductor with an energy gap of 3.37 eV while TiO_2 is an indirect band

* Corresponding author at: Laboratory of Inorganic Materials Chemistry, University of Namur, Namur, Belgium and State Key Laboraory of Advanced Technology for Materials Synthesis and Processing, Wuhan University of Technology, Wuhan, China.
** Corresponding authors.
E-mail addresses: minwu@whut.edu.cn (M. Wu), yu.li@whut.edu.cn (Y. Li), bao-lian.su@unamur.be, baoliansu@whut.edu.cn, bls26@cam.ac.uk (B.-L. Su).
http://dx.doi.org/10.1016/j.apcatb.2016.06.016
0926-3373/

gap one with energy gap of 3.2 eV [4,5]. Both ZnO and TiO_2 have good optical properties and good photocatalytic activity in the UV region. However, their photocatalytic efficiency is still relatively low due to the fast recombination of photoinduced charge carriers [6]. Many strategies have been developed in order to improve the photocatalytic efficiency of TiO_2 through doping with a second component which promotes photon-to-electron conversion efficiency and charge separation. It is now well recognized that the photocatalytic activity of TiO_2 nanoparticles depends not only on the properties of the TiO_2 material itself, but also on the performance of the modified material [7–9]. A lot of researches have shown that the photocatalytic activity of TiO_2 and ZnO can be effectively improved by doping them with semiconductors such as ZnO/TiO_2 which may provide another alternative to solve the problem of fast electron-hole recombination [10–13]. A nanocomposite made of ZnO and TiO_2 seems to be useful in achieving more efficient generation of electron/hole pairs under UV illumination and also in obtaining higher reaction rates as compared to other semiconductor couples [14–16]. The enhanced photocatalytic activity of coupled ZnO/TiO_2 particles in comparison with pure ZnO and TiO_2 alone has been largely studied [17–24] and the results show that ZnO/TiO_2 nanocomposites not only improve the photogeneration efficiency, but also suppress the recombination of photogenerated electron/hole pairs. Thus, coupled ZnO/TiO_2 semiconductors are a good approach to achieve a more efficient charge separation, an increased lifetime of the charge carriers, and an enhanced interfacial charge transfer to adsorbed substrates [25].

Photocatalytic efficiency of the ZnO/TiO_2 system was evaluated in terms of degradation of pollaunts such as Rhodamine B (RhB) aqueous solution. RhB, a xanthene dye is widely used as a colorant in textiles and also a well-known water tracer fluorescent. During the photocatalytic process, the dye molecules are adsorbed on the surface of the catalysts, where chemical bonds are broken and small organic molecules are released as decomposed products. When the photocatalyst is irradiated in the presence of water hydroxyl radicals $OH^{\cdot}$, as strong oxidant agent, are photogenerated. These reactive species are able to achieve a complete mineralization of organic dyes. Rhodamine B (RhB) is a common dye in the triphenylmethane family, which contains four *N*-ethyl groups at either side of the xanthene ring. It has been reported that in the visible-light induced photocatalytic degradation of RhB, as *N*-ethyl-containing dye, three main steps, namely *N*-deethylation, cleavage of chromoporme and mineralization of dye, were frequently witnessed [26–28]. At the end of photocatalytic process, the RhB dye is completely mineralized into CO_2, H_2O [29–34].

Recently, as a novel method among many surface modification techniques used to improve the lifetime of photogenerated electron-hole pairs, semiconductor quantum dots (QDs) have been widely used to sensitize photocatalysts such as CdS QDs/TiO_2, CdTe QDs/ZnO and Bi_2S_3 QDs/TiO_2 [35–37]. The quantum size effect in semiconductor QDs has already been reported to have a great influence on the photocatalytic activity of QDs based photocatalysts [38–43]. Zinc oxide is one of the few oxides that exhibit quantum confinement effects. One important consequence of the quantum size effect in semiconductor photocatalysts is that the reduced size of nanoparticles directly affects exciton properties through the increase of the surface to volume ratio, which leads to an enhancement of the access of electrons and holes to the surface, and therefore to more efficient oxidation and reduction processes. Another important consequence of the quantum size effect is the rapid diffusion of photogenerated charges to the surface of the nanoparticles due to the increase of the forbidden band gap width, and the ability of the semiconductors to accumulate high densities of excess charges which can help to overcome the potential barrier of the photoreductive chemical process. As a result, the photocatalytic activity is considerably enhanced. Ramakrishna et al. [44] demonstrated that the quantum yield of phototransfer of a hole from the valence band of ZnO nanoparticles to various phenols increases by an order of magnitude with a decrease of the particle size from 4.2 to 3.2 nm. The electronic energy levels of QDs can be varied by altering their dimensions, and thus their effective bandgap can be tuned to maximize the absorption of the solar spectrum. Moreover, these levels can be shifted in order to control charge transfer across heterointerfaces [45].

Few reports have focused on the photocatalytic activity of binary compounds based on quantum dots coupled with TiO_2 photocatalysts. Huang et al. [46] found that the photocatalytic activity of TiO_2 was significantly enhanced after incorporation of CdS QDs. Yu et al. [47] reported that quantum-sized CdSe nanoparticles enhanced the photocatalytic activity of the CdSe/TiO_2 coupled system in the degradation of 4-chlorophenol (4-CP) due to the high surface-to-volume ratio of quantum dots and the promotion of charge carrier separation. In addition, it has been revealed that TiO_2 photocatalysts coupled with quantum-sized MoS_2 and WS_2 nanoclusters exhibited an enhanced visible light activity in the degradation of methylene blue (MB) and 4-chlorophenol [48]. The quantum size effect (QSE) alters the energy levels of the conduction and the valence band edges in the coupled semiconductor systems, which favors the interparticle electron transfer resulting in low carrier recombination rate. Xie et al. [49] showed that CdS QDs sensitized TiO_2 nanotubes exhibited high photocatalytic activity towards methyl orange (MO) dye due to the quick charge transfer from CdS to TiO_2 conduction band. Another important work carried out by Wang et al. [50] showed clearly the QSE in photocatalysis. It has been found that CdSe QDs-modified TiO_2 performed much better than both pure TiO_2 and bulk CdSe modified-TiO_2 towards degradation of malachite green (MG) under visible light irradiation. The quantum size effect leads to an enlargement of the band gap. In contrast to bulk CdSe-modified TiO_2, the larger difference between the conduction band potentials of CdSe QDs and TiO_2 greatly increases the electron transfer rate from CdSe QDs to TiO_2, which is beneficial for efficient charge carrier separation.

Very recently, because of their applications in catalysis, much interest has been devoted to three dimensionally ordered macroporous (3DOM) materials with pore sizes in the sub-micrometer range [51–53]. Note that 3DOM materials belong to the more general class of photonic crystal materials. 3DOM TiO_2 has been recognized as an efficient photocatalyst due to its unique properties in terms of uniformly ordered and interconnected macroporous architecture. The presence of macropores provides easy mass transfer of the reactant molecules and accessibility to the active sites, large surface area, and enhanced light absorption owing to multiple scattering and slow photons [42–44]. Therefore, compounds based on 3DOM TiO_2 are considered as the most promising catalytic materials. Zheng et al., in a recent article [54], synthesized a highly ordered ZnO/TiO_2 photonic crystal (PC) heterostructure nanocomposite with enhanced photocatalytic properties. According to this work, the high photocatalytic activity of ZnO/TiO_2-PC nanocomposite, compared with ZnO, TiO_2-PC and commercial P25 titania catalysts, can be attributed to the formation of an intimate heterojunction structure at the interface between ZnO particles and TiO_2-PC, which greatly promotes the separation of photogenerated electron-hole charge carriers. In addition, the ZnO/TiO_2-PC as an hybrid system possesses excellent photostability and could be readily recovered owing to the periodic photonic structures of ZnO/TiO_2-PC. It was found that the presence of inverse opal structure in the ZnO/TiO_2 nanocomposite could effectively facilitate the separation of electron-hole pairs, which might generate more radical species with strong oxidation capability for dye degradation. A 3DOM Ag/ZnO–TiO_2 composite was synthesized via a sol–gel method by Li et al. [55] who found that this composite displayed excellent photocatalytic activity towards the degrada-

tion of different organic pollutants using UV light irradiation, compared to that of P25, ZnO, and Ag/ZnO–TiO_2. The uniformly ordered macroporous structure of Ag/ZnO–TiO_2 composite provided more active sites for the intake and outtake of pollutant molecules. Moreover, the diffraction of light by the regular pore array and the porous structure of the material have a synergistic effect on the optical absorption. As a result, the efficiency of 3DOM Ag/ZnO–TiO_2 composite for degradation of organic pollutants was significantly improved. More importantly, uniformly ordered macroporous materials with pore size in the optical wavelength range can produce peculiar optical effects which enhance the efficiency of light energy conversion [52,53,56–58], being beneficial for photocatalysis [59–64].

In this work, the benefits of light sensitization and quantum size effects of ZnO QDs and the advantage of photonic structure and high surface accessibility of 3DOM TiO_2 are for the first time combined together to construct ZnO QDs@3DOM TiO_2. Such nanocomposites with intimate contact were prepared by the sol gel method combined with a polysterene (PS) latex sphere templating technique. It is expected that the formation of an intimate heterojunction between ZnO nanoparticles and 3DOM TiO_2 can highly favor the separation of photo-induced electron-hole pairs and guarantee the symbiose phenomenon of QDEs and slow light effect of 3 DOM TiO_2 photonic crystal. The QDEs of ZnO nanoparticles induce two important consequencies: (1) ZnO nanoparticles absorbs strongly light and plays a very important sensitizor effect to capture of the light; (2) QDEs of ZnO nanoparticles result in an increase in the width of the forbidden electronic band which increases the energy of electrons (holes) in the conduction (valence) band and particularly leads to a displacement of the conduction band potentials of ZnO to more negative energy levels compared to TiO_2, favoring therefore significantly the separation in space the electron-hole pairs. The light sensitizing effect of ZnO nanoparticles can amplify the slow light effect generated by 3DOM TiO_2 due to its photonic structure. Thus the ZnO QDs@3DOM TiO_2 nanocomposites could exhibit a greatly enhanced photocatalytic activity towards the degradation of RhB under UV irradiation, due to higher photogenerated charge energy and quicker charge transfer, photonic optical properties and to the high accessibility of 3DOM structure. The vital role that QSE plays combining with 3DOM photonic optical properties in enhancing photocatalytic properties of ZnO QDs/3DOM TiO_2 nanocomposites is discussed.

2. Experimental

2.1. Synthesis of colloidal ZnO QDs

Colloidal ZnO nanoparticles were prepared by hydrolyzing zinc acetate dehydrate in the basic methanol solution. In a typical synthesis, 0.1 M zinc acetate solution and 1 M KOH solution were prepared, respectively, by dissolving 0.55 g of zinc acetate in 25 ml of methanol and by dissolving 2.8 g of KOH in 50 ml methanol. The reaction was carried out at room temperature by dropwise addition of KOH solution to zinc acetate solution with constant stirring. The final pH of the solution was maintained at 10. The resulting solution was homogenized by stirring continuously for 1 h with a magnetic stirrer. At this stage, 0.25 ml of tetraethylorthosillicate (TEOS) solution was added into the ZnO solution to control particle growth. Immediately after this, 0.5 ml of distilled water was injected to the colloidal solution for mild sol–gel reaction of silica on particle surfaces. The as-prepared colloid was separated by centrifuging and washed several times by methanol followed by distilled water to remove unreacted molecules. Finally, the as-obtained colloid was dispersed in water medium (12 mg/ml) and pure ZnO QDs were obtained [65].

2.2. Synthesis of sol-gel ZnO QDs@TiO_2

Firstly, a TiO_2 sol–gel precursor was prepared by mixing ethanol, hydrochloric acid, titanium (IV) isopropoxide and water followed by being mixed with ZnO QDs solution; 1 mg/ml, 1.5 mg/ml and 2 mg/ml, respectively. Finally, ZnO QDs@TiO_2 sol-gel solutions were ready for usage.

2.3. Fabrication of ZnO QDs@3DOM TiO_2 nanocomposites

The fabrication of three dimensionally ordered macroporous (3DOM) titania was achieved via a templating strategy, according to our previous report [63]. Using the same strategy, ZnO QDs@3DOM TiO_2 was synthesized. A thick layer of self-assembled polystyrene spheres (PS), with average pore size of about 370 nm, was deposited onto a filter paper in a Buchner funnel under vacuum. The PS template was then infiltrated with the ZnO QDs@TiO_2 precursor solution. After air drying for 24 h, the precursor-template mixture was calcined at 550 °C for 12 h to obtain ZnO QDs@3DOM TiO_2 photonic crystal (PC) with inverse opal structure (IOS), in the form of a powder. ZnO QDs@ 3DOM TiO_2 nanocomposites with different ZnO/TiO_2 ratios: 0.026, 0.04, and 0.052 were prepared and labelled as 0.026ZnO QDs@3DOM TiO_2, 0.04ZnO QDs@3DOM TiO_2 and 0.052ZnO QDs@3DOM TiO_2, respectively. A 0.052 ZnO/3DOM TiO_2 (0.052ZnO@3DOM TiO_2) nanocomposite was synthesized via the wetness impregnation method by mixing aqueous solution of $Zn(NO_3)_2$ with the as prepared 3DOM TiO_2.

2.4. Characterization

The crystalline structure of the so-obtained powder samples was characterized by powder X-ray diffraction (XRD) (a PANalytical X'pert Pro with Cu Ka radiation). The morphological properties of the samples were observed by scanning electron microscopy (SEM) (Jeol JSM-7500F) and a field emission scaning microscopy (FESEM Hitachi S-4800) equipped with an energy dispersive X-ray detector (EDX). Furthermore, transmission electron microscopy (TEM) was performed on a Philips FEI-Tecnai 10 electron microscope with an accelerating voltage of 80 kV. X-ray photoelectron spectroscopy (XPS) analysis was performed on a K-Alpha TM + X-ray photoelectron spectrometer (XPS). The binding energy for the C (1s) peak at 284.9 eV, (relative to adventitious carbon from the XPS instrument itself), was used as a reference. Textural properties of the materials were evaluated via adsorption–desorption of nitrogen at −196 °C using a Micromeritics Tristar 3000 with prior outgassing. The UV–vis absorbance spectra were obtained using a UV–vis spectrophotometer (Perkin Elmer Lambda 35 UV–vis spectrometer fitted with a Labsphere for analysis in diffuse reflectance mode) in the range of 200–750 nm. Photoluminescence properties of the samples were studied by PerkinElmer LS45 luminescence spectrometry.

2.5. Photocatalytic testing

Photocatalytic testing was performed under UV irradiation ($\lambda < 400$ nm) using 6 neon lamps of 18 W. The luminous power of each lamp was 1250 lm and the total luminous power was 7500 lm in the photocatalytic reactor at room temperature. For each experiment, 20 mg of the photocatalyst was placed in 50 ml of reactant solution with an initial concentration of 10–3 M of RhB. The suspension was poured into a quartz tube, inserted into the reactor and stirred in the dark for 60 min to ensure adsorption/desorption equilibrium prior to irradiation. During irradiation, 2 ml of the suspension was removed at a given time interval for subsequent RhB concentration analysis.

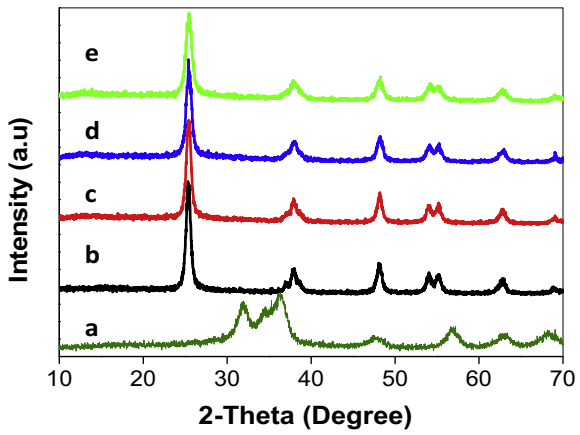

Fig. 1. XRD patterns of ZnO QDs powder (a), 3DOM TiO_2 (b), 0.026ZnO QDs@3DOM TiO_2 (c), 0.04ZnO QDs@3DOM TiO_2 (d) and 0.052ZnO QDs/3DOM TiO_2 (e) nanocomposites.

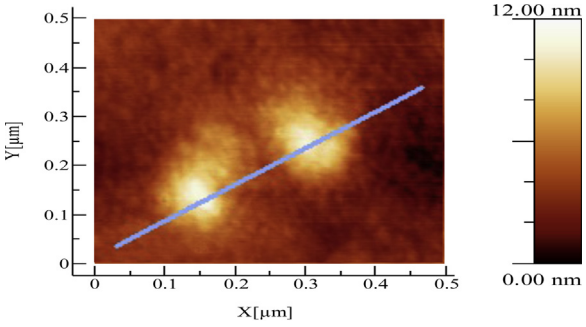

Fig. 2. Atomic force microscopic image of ZnO QDs.

3. Results and discussions

3.1. Phase composition

The XRD patterns of the as-synthesized ZnO QDs, 3DOM TiO_2 and three ZnO QDs@3DOM TiO_2 nanocomposites, as shown in Fig. 1, revealed well crystallized samples. The XRD pattern of ZnO QDs (Fig. 1a) shows seven peaks corresponding to the crystal planes (100), (002), (101), (102), (110), (103) and (200) which indicate that the obtained ZnO particles crystallized into the hexagonal Wurtzite phase (JCPDS 36-1451). The obviously broadened diffraction peaks clearly show that very small nanoparticles were obtained. The average crystallite size is about 5.5 nm as determined by the Debye–Scherrer equation given by [66]:

$$D = k\lambda/\beta\cos\theta$$

where D is the crystal size, λ is the wavelength, K is a constant, β is the peak widths at half-maximum intensity (FWHM) for ZnO (100) and (101) peaks, and θ is the corresponding Bragg's diffraction angle.

The ZnO quantum dot size in ZnO QDs@3DOM TiO_2 solution was further studied by Atomic Force Microscopy and gives a size around 5–6 nm (Fig. 2) in good accordance with XRD resuls.

The XRD pattern of the as-synthesized TiO_2 inverse opal structure (Fig. 1b) shows five peaks at 2θ = 25.3°, 37.9°, 48.0°, 54.6° and 62.8° corresponding to the crystal planes of (101), (004), (200), (211), and (204), respectively (JCPDS card no. 14-0688), which indicate that TiO_2 crystallized into the anatase phase. Fig. 1c–e show the XRD patterns of the ZnO QDs@3DOM TiO_2 nanocomposite samples. It is found that all of the X-ray diffraction peaks are indexed to anatase phase of TiO_2, showing that the introduction of ZnO QDs does not change the lattice structure of TiO_2. No shift of the principal peaks of TiO_2 in the ZnO QDs@3DOM TiO_2 nanocomposites is observed further confirming that the prepared samples are highly crystallized which is essential for a good photocatalytic material. Moreover, no diffraction peaks assigned to ZnO QDs are found, which could be ascribed to the small amount of ZnO QDs, the particle size in nanoscale

and their high dispersion in 3DOM TiO_2. The same result was found by Wang et al. for their CdSe quantum dots-modified TiO_2 samples [50]. The average crystallite sizes of TiO_2 nanoparticles in pure TiO_2 inverse opal structure and in 0.026ZnO QDs@3DOM TiO_2, 0.04ZnO QDs@3DOM and 0.052ZnO QDs@3DOM TiO_2 nanocomposites calculated from the TiO_2 (101) peak by using the Debye–Scherrer formula, were found to be 11.8, 10.3, 8.5 and 7.2 nm, respectively. The crystallite size of TiO_2 decreases as the amount of ZnO QDs in 3DOM TiO_2 increases. These results reveal that the incorporation of ZnO QDs could effectively inhibit the growth of TiO_2 crystallites. This fact could be associated to a slightly decrease in the sample crystallinity due to the ZnO QDs. It is well known that the addition of a second component to a metal oxide can inhibit or at least delay the crystallization of the metal oxide due to nanocomposite effect [67]. The crystallization of the metal oxide will occur at higher temperatures. The accumulation of ZnO QDs on the external surfaces of TiO_2 could thus hinder TiO_2 crystal growth. With increasing the ZnO QDs content in the nanocomposite, this effect is reinforced. The TiO_2 nucleation occurs at high temperature and thus TiO_2 nanoparticle size decreases.

3.2. Morphology

Fig. 3 shows SEM images of pure TiO_2 inverse opal (a) and ZnO QDs@3DOM TiO_2 nanocomposites with different compositions (b–d). It can be clearly seen that all samples displayed high quality of three dimensional ordered inverse opal structures. The underlying layer of pores and porous walls can also be easily observed, indicating that the samples possess a three dimensionally well-open, ordered and interconnected macroporous network. The average pore size is about 350 nm, being smaller than the size of PS spheres used for the preparation of opal template due to the thermal contraction.

The elemental composition of ZnO QDs@3DOM TiO_2 was analyzed by energy dispersive X-ray spectroscopy (EDS). As shown in Fig. 4, the EDX mapping of 0.052ZnO QDs@3DOM TiO_2 indicated the presence of Zn, Ti and O atoms (Fig. 4b and c and d, respectively) in the sample. Fig. 4e shows a highly homogenous dispersion of the ZnO QDs (red color) in the 3DOM TiO_2.

Fig. 5 shows the TEM and HRTEM images of 0.052ZnO QDs@3DOM TiO_2 as representative image of all the samples. It is clearly seen that this nanocomposite possessed a high-quality 3DOM structure (Fig. 5a and b) which was composed of interconnected macropores within a nanocrystalline skeleton, in good agreement with the SEM observations. HRTEM image (Fig. 5c) shows the presence of ZnO QDs with a particle size of 5–10 nm while particle size of TiO_2 is around 5–15 nm.

3.3. XPS analysis

The X-ray photoelectron spectroscopy (XPS) measurements were carried out for the as-prepared samples to determine the surface composition and oxidation states of the elements. The survey spectra of 0.052ZnO QDs@3DOM TiO_2 nanocomposite, 3DOM TiO_2 and pure ZnO QDs are shown in Fig. 5(a). The ZnO QDs@3DOM TiO_2 nanocomposite is mainly composed of four principal elements, i.e., C1s, O1s, Ti2p, and Zn2p. Fig. 6(b)–(d) show the high resolution spectra of Ti2p, Zn2p and O1 s in the 0.052ZnO QDs@3DOM TiO_2 nanocomposite as well as in pure ZnO QDs and 3DOM TiO_2 for com-

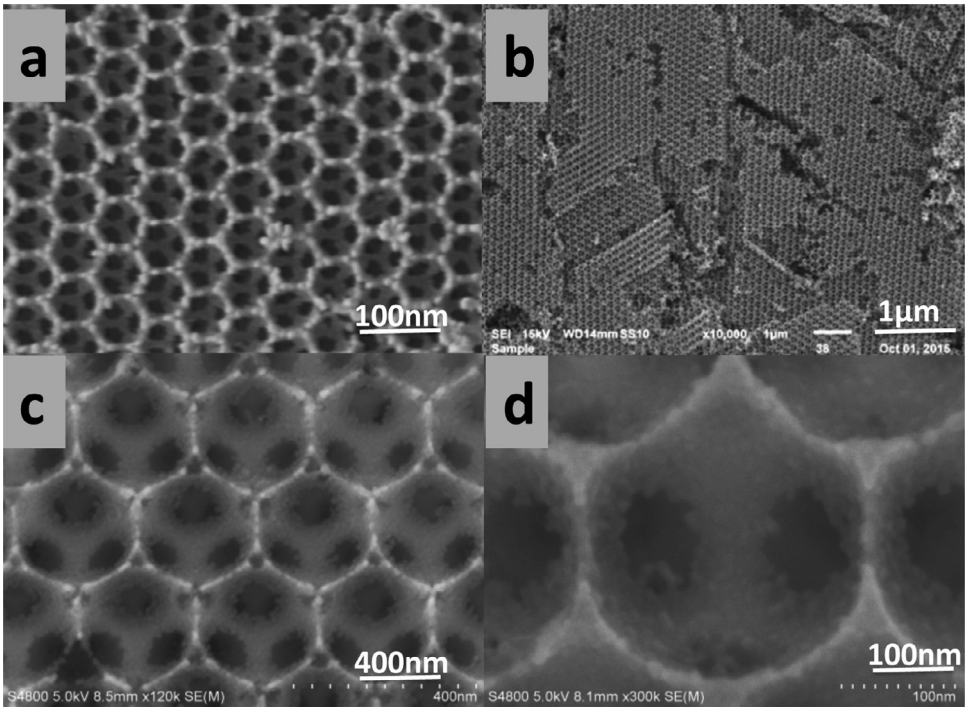

Fig. 3. SEM images of (a) 3DOM TiO_2, and (b)-(d) 0.052ZnO QDs@3DOM TiO_2 photocatalysts at different magnifications.

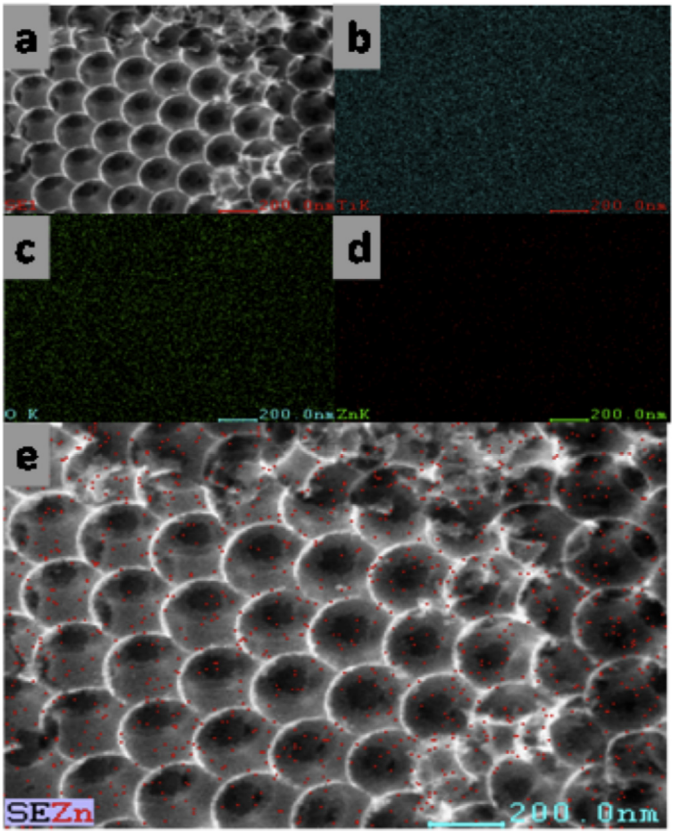

Fig. 4. EDX mapping spectra of 0.052ZnO QDs@3DOM TiO_2 nanocomposite. (a) SEM picture of mapping zone, (b) mapping of Ti element, (c) mapping of O element, (d) mapping of Zn element and (e) Dispersion of Zn element on 3DOM TiO_2 (picture obtained by combining (a) and (d), red dots represent ZnO QDs). (For interpretation of the references to colour in this figure legend, the reader is referred to the web version of this article.)

parison. As can be seen in Fig. 6(c), the XPS spectrum of Zn2p reveals two peaks located at 1022.4 eV and 1045.5 eV, corresponding to Zn 2p3/2 and Zn 2p1/2, respectively. The spin-orbit splitting of Zn2p with 23.1 eV indicated that Zn ions mainly existed as Zn^{2+} in ZnO as reported in the literature [68]. Compared with pure ZnO QDs, a shift of 1.1 eV in the peak positions of ZnO (1021.3 eV and 1044.4 eV) is observed, confirming the possible charge transfer between ZnO and TiO_2. The XPS spectrum of Ti depicts a doublet with peaks centered at 459.2 eV and 464.9 eV, which correspond to the Ti2p3/2 orbit and Ti2p1/2 orbit, respectively. The spectral separation between Ti 2p3/2 and Ti2p1/2 peaks is 5.7 eV, which corresponds to the expected oxidation state of Ti^{4+} [69]. Compared with 3DOM TiO_2, a shift of 0.4 eV is also observed in the position peaks corresponding to Ti2p (458.8 eV for the Ti 2p3/2 orbit and 464.5 eV for Ti2p1/2). The XPS spectrum of oxygen shows that the binding energy of O1 s on the ZnO QDs@3DOM TiO_2 nanocomposite has shifted to about 530.5 eV compared with 3DOM TiO_2 at 530 eV, due to the fact that the binding energy of O_2 in ZnO lattice is located at higher position of 530.8 eV as compared with one for 3DOM TiO_2. The fact that Ti2p, Zn2p and O1s peaks positions in the ZnO QDs@3DOM TiO_2 nanocomposite had slight shift compared with those in pure ZnO QDs and 3DOM TiO_2 samples indicates that a charge or energy transfer occurred after the formation of the heterojunction.

3.4. Optical properties

In order to characterize the optical properties of as synthesized samples, UV–vis absorbance spectra of ZnO QDs, 3DOM TiO_2, 0.026ZnO QDs@3DOM TiO_2, 0.04ZnO QDs@3DOM TiO_2 and 0.052ZnO QDs@3DOM TiO_2 nanocomposites were measured (Fig. 7). As can be seen from the linear fitting to replotted curve labelled a in the insert, the colloidal ZnO QDs show an absorption edge at 3.56 eV. From the absorbance spectra of the ZnO QDs@3DOM TiO_2 nanocomposites (curves c,d), it can be observed that, as the ZnO QDs content increases, the optical absorption edges are shifted to higher energies, compared with that of TiO_2 (curve b), which can be related to the quantum size effect.

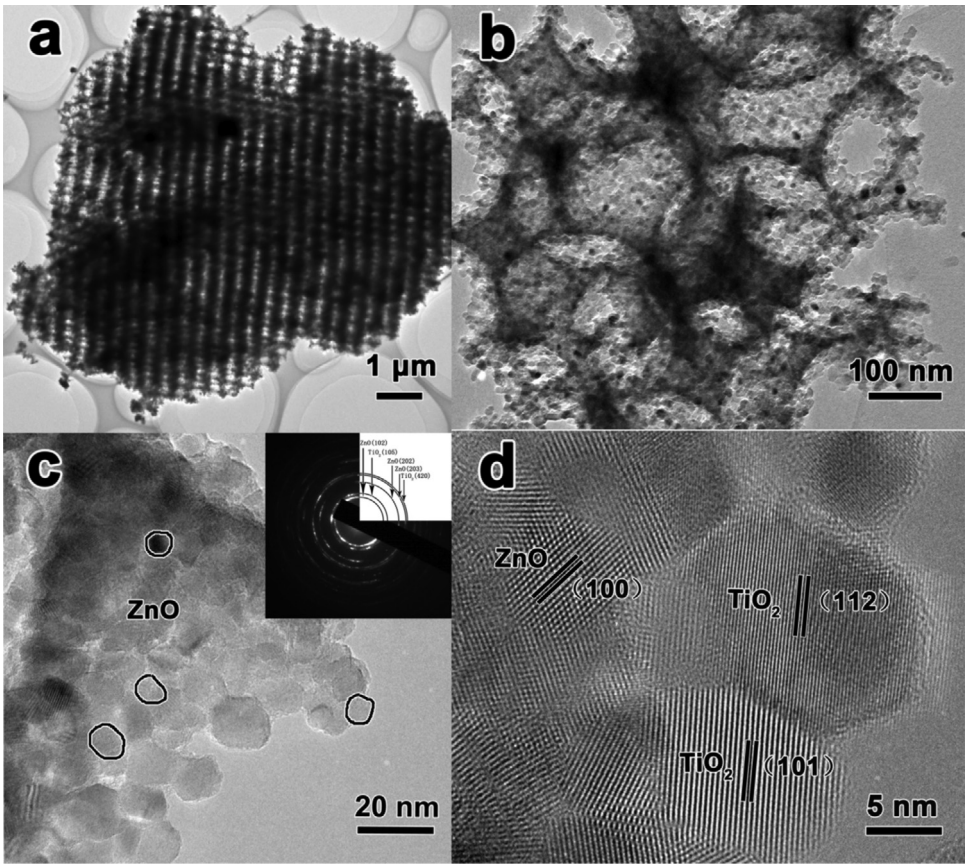

Fig. 5. TEM (a and b) and HRTEM (c and d) images of 0.052ZnO QDs@3DOM TiO_2 photocatalyst. Inset of (c) is the electron diffraction.

The optical band gap energy can be estimated from the so called Tauc's plots defined by the linear equation $(\alpha h\nu)^{1/2} = A\,(h\nu - E_g)$, where α, h, A, ν and E_g are, respectively, the absorption coefficient near the absorption edge, the Planck constant, a constant, the frequency of light and the absorption band gap energy. The plots of $(\alpha h\nu)^{1/2}$ versus the photon energy ($h\nu$) and the corresponding linear fitting are shown in the insert for each sample. The band gap of colloidal ZnO QDs, 3DOM TiO_2 and TiO_2 nanoparticles in 0.026ZnO QDs@3DOM TiO_2, 0.04ZnO QDs@3DOM TiO_2 and 0.052ZnO QDs@3DOM TiO_2 nanocomposites are estimated to be about 3.51 eV, 3.11 eV, 3.18 eV, 3.21 eV and 3.24 eV, respectively.

Fig. 8. shows that the fabricated materials are iridescent, which indicates a well-organized 3DOM structure. It is interesting to note that, as the amount of ZnO QDs in 3DOM TiO_2 increases, the color of ZnO QDs@3DOM TiO_2 nanocomposites changes: yellow for the 3DOM TiO_2 inverse opal structure, red for the 0.026ZnO QDS@3DOM TiO_2, violet-red for the 0.04ZnO QDS@3DOM TiO_2 and blue-green for the 0.052ZnO QDS@3DOM TiO_2 nanocomposites. The yellow iridescence is due to the positioning of the photonic band gap of the TiO_2 inverse opal in the middle of the visible range, as in measurement of the reflectance spectra (not shown). Because the absorption edge of TiO_2 is close to the shorter wavelength side of the visible range, it may slightly influence the reflectance and modify the color that would result from the photonic band gap in the absence of material absorption. Since the incorporation of increasing amount of ZnO QDs resulted in a shift of the absorption edge towards shorter wavelengths (Fig. 6), the colors of ZnO QDs@3DOM TiO_2 nanocomposites were modified accordingly. Because of the non-trivial interplay between photonic band gap and material absorption properties, numerical simulations of the reflectance spectrum of the ZnO QDs@3DOM TiO_2 nanocomposites would be required for quantitative assessment of the colors.

The photoluminsecence (PL) emission spectra can supply meaningful information about semiconductor materials such as surface oxygen or metal vacancies, the efficiencies of charge carrier migration and transfer, and it is quite helpful to understand the recombination rate of electron-hole pairs in semiconductor as PL emission arises from the recombination of free carriers [70,71].

Fig. 9 presents the PL spectra of the as-prepared samples. Colloidal ZnO QDs (spectrum a) exhibits a strong green emission located at 530 nm mainly caused by oxygen vacancy defects [72–74]. The pure TiO_2 inverse opal structure (spectrum b) gives a strong PL signal in the range of 400–450 nm, with four obvious PL peaks at about 442, 460, 493 and 525 nm, respectively, possibly the first one mainly resulting from band edge free excitons and the fourth one mainly from binding excitons [75,76]. All ZnO QDs@3DOM TiO_2 nanocomposites (spectra c–e) exhibit four PL emission peaks located at 390, 420, 486 and 530 nm, respectively. The UV emission located at 390 nm is generally attributed to the recombination of free excitons of ZnO [77].

Compared with 3DOM TiO_2 the disappearance of the peak located at 410 nm after the introduction of ZnO indicates that the recombination rate decreases after the formation of the nano-heterojonction. Additionally, the PL intensity of ZnO QDs@3DOM TiO_2 decreases as the ZnO QDs amount increases. It is well known that PL emission results from the recombination of excited charge carriers and there is a strong correlation between PL emission intensity and photocatalytic performances [78,79]. Generally, the lower PL intensity suggests a lower recombination rate of photogenerated electron-hole pairs, which leads to a higher photocatalytic activity of semiconductor photocatalysts [80]. Compared to other samples, the 0.052ZnO QDs@3DOM TiO_2 (spectrum e) exhibits the lowest PL emission intensity which suggests that it pos-

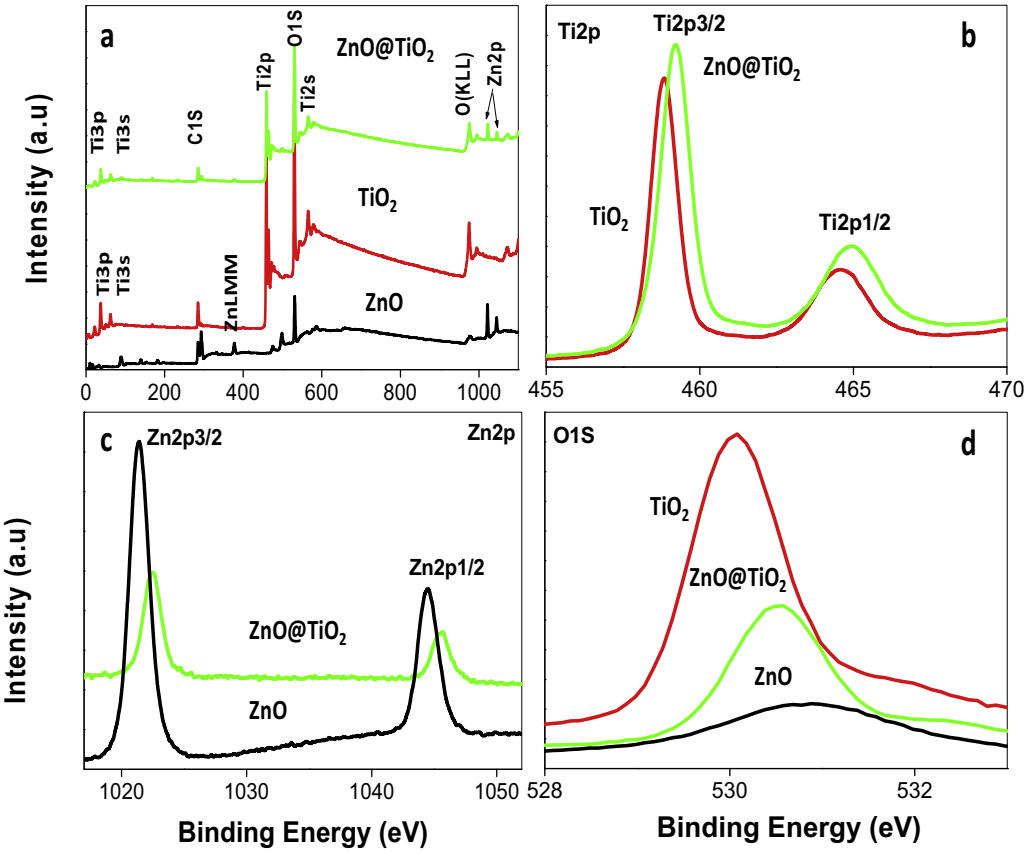

Fig. 6. (a) Wide scan survey XPS spectra of ZnO QDs, 3DOM TiO_2 and 0.052ZnO QDs@3DOM TiO_2 nanocomposite. High-resolution XPS spectra of Ti 2p (b), Zn 2p (c) and O 1s (d) regions.

sesses the highest separation efficiency of charge carriers, resulting in the highest photocatalytic activity.

3.5. Textural properties

Fig. 10 shows the nitrogen adsorption-desorption isotherms and pore size distribution curves of 3DOM TiO_2 and ZnO QDs@3DOM TiO_2 nanocomposites with different compositions. The isotherms of all samples were of type II with a H3 hysteresis loop in the relative pressure (p/p_o) range of 0.9-1.0 [81] indicating the presence of a macroporous structure [82,83] which was also confirmed by the SEM and TEM observations. A BET surface area of 26 m^2/g was found for the 3DOM TiO_2 sample. After loading with ZnO QDs, this value increased to 33, 35 and 37 m^2/g for the 0.026ZnO QDs@3DOM TiO_2, 0.04ZnO QDs@3DOM TiO_2 and 0.052ZnO QDs@3DOM TiO_2, respectively due to the additional contribution of high surface areas of ZnO QDs. All 3DOM samples exhibited a narrow pore size distribution. The samples possessed a pore-size distribution centered at 2, 1.7, 1.5 and 2.2 nm, for the 3DOM TiO_2, 0.026ZnO QDs@3DOM TiO_2, 0.04ZnO QDs@3DOM TiO_2 and 0.052ZnO QDs@3DOM TiO_2, respectively, mainly due to the aggregation of TiO_2 nanoparticles. For three ZnO QDs@3DOM TiO_2 nanocomposites (Fig. 10(b)–(d)), a second pore size centered at 2.6, 3.0 and 3.2 nm, respectively, appeared and could be attributed to the aggregation of ZnO nanoparticles. As for the pore volume, it increased with the addition of increasing amount of ZnO QDs.

For the sake of facility, all the physicochemical properties of studied photocatalysts are summarized in Table 1.

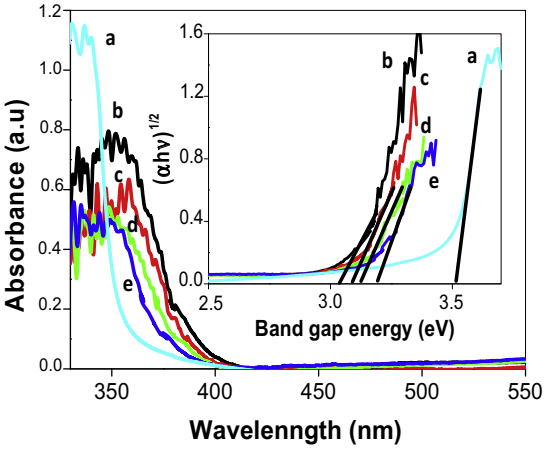

Fig. 7. UV–vis absorbance spectra of (a) pure colloidal ZnO QDs, (b) pure inverse opal structure TiO_2, (c) 0.026ZnO QDs@3DOM TiO_2, (d) 0.04ZnO QDs@3DOM TiO_2 and (e) 0.052ZnO QDs@3DOM TiO_2 nanocomposites. Insert: linear fitting to Tauc's replotted curves: the intersection of the straight lines with the x-axis gives the band gap energy.

3.6. Photocatalytic activity

The photocatalytic activity of the as-prepared samples was evaluated by monitoring the degradation of RhB in aqueous solution under UV light irradiation at room temperature. Fig. 11 shows the photocatalytic efficiencies (C/C_0) of 3DOM TiO_2, ZnO QDs@3DOM TiO_2 nanocomposites with different compositions, where C and C_0 are the initial concentration (after equilibrium) and the reaction

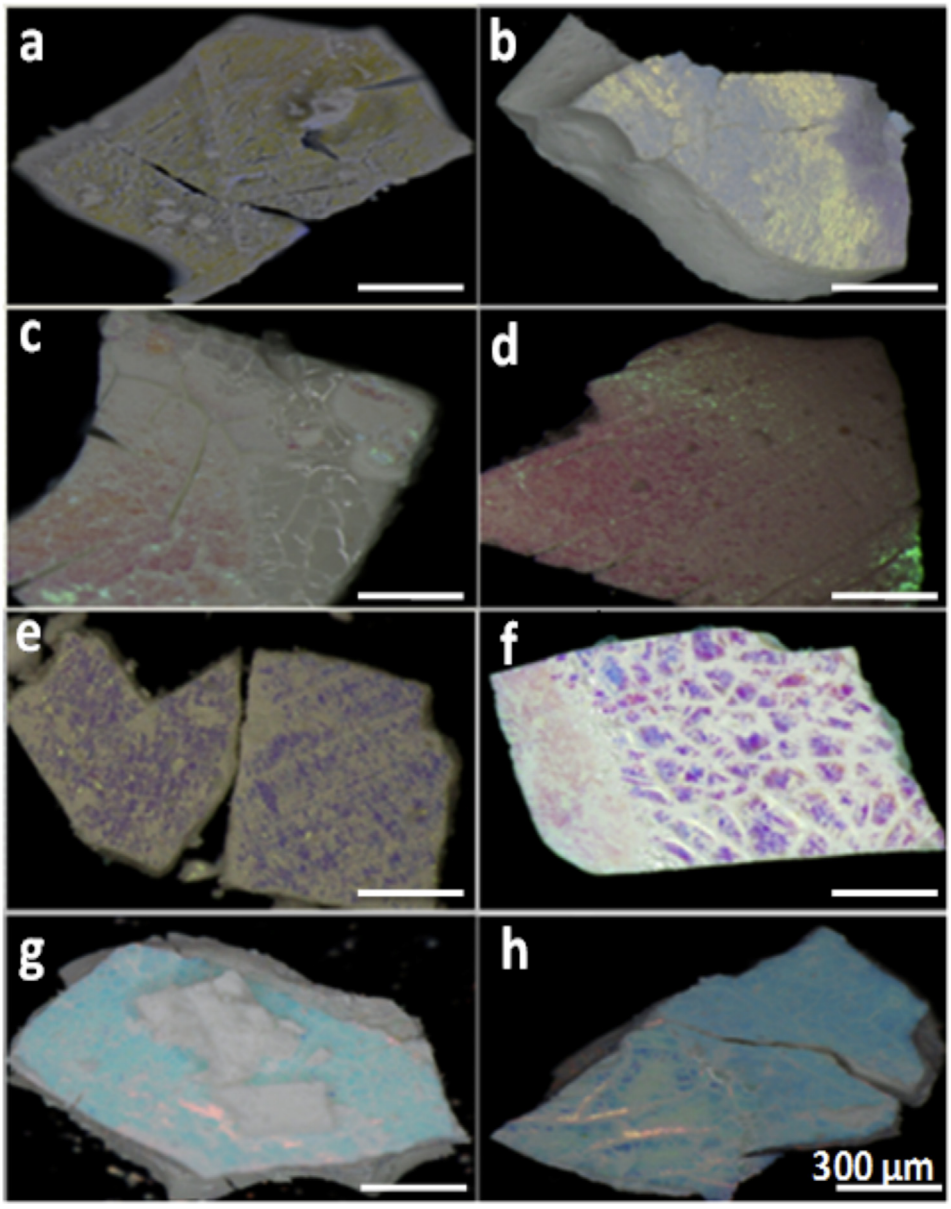

Fig. 8. Optical images of 3DOM TiO_2 (a) and (b), 0.026ZnO QDs@3DOM TiO_2 (c) and (d), 0.04ZnO QDs@3DOM TiO_2 (e) and (f), and 0.052ZnO QDs@3DOM TiO_2 (g) and (h).

Table 1
Physico-chemical properties of studied photocatalysts.

Samples	S_{BET} (m^2/g)	Pore sizes (nm) (Bimodal)	TiO_2 crystallite size (nm, XRD/TEM)	Band gap of photocatalysts (eV)
ZnO QDs	–	–	–	3.51
3DOM TiO_2	26	2.0/–	11.8/10–25	3.11
0.02ZnO QDs@3DOM TiO_2	33	1.7/2.6	10.3/8–20	3.18
0.04ZnO QDs@3DOM TiO_2	35	1.5/3.0	8.5/5–20	3.21
0.052ZnO QDs@3DOM TiO_2	37	2.2/3.2	7.2/5–15	3.24

concentration of RhB, respectively. A blank test, i.e. without the addition of the photocatalyst, was made and a little decrease in the concentration of RhB of about 12% was found after 60 min. Moreover, P25 was taken as reference for comparison purpose and, in this case, the RhB degradation was about 70% after 60 min. For the 3DOM TiO_2 sample, the photodegradation of RhB reached to about 100% after 60 min.

As for ZnO QDs@3DOM TiO_2 nanocomposites, the RhB degradation rate increased as the ZnO QDs content increased. The photodegradatrion of RhB was about 100% with 0.026ZnO QDs@ 3DOM TiO_2 and 0.04ZnO QDs@3DOM TiO_2 after 45 min. The 0.052ZnO QDs@3DOM TiO_2 exhibited the best photocatalytic activity with RhB completely degraded only after 30 min. For comparison a 0.052 ZnO/3DOM TiO_2 nanocomposite was synthesized via the wetness impregnation method by mixing aqueous solution of $Zn(NO_3)_2$ with the as prepared 3DOM TiO_2. The size of ZnO was about 19 nm. The photodegradation of RhB was about 100% after 60 min. The photodegradation performances of RhB can be ranked by decreasing order of the activity as follows: 0.052ZnO QDs@3DOM TiO_2 > 0.04ZnO

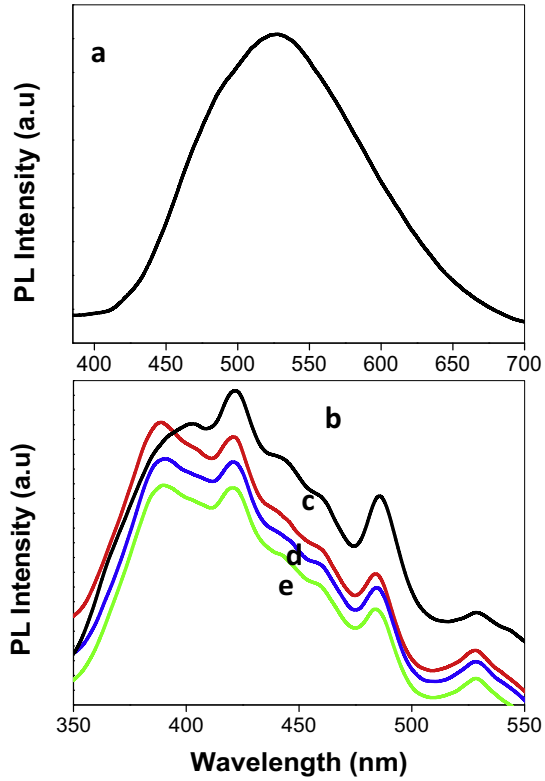

Fig. 9. Photoluminescence (PL) spectra of (a) colloidal ZnO QDs, (b) 3DOM TiO_2, (c) 0.026ZnO QDs@3DOM TiO_2, (d) 0.04ZnO QDs@3DOM TiO_2 and (e) 0.052ZnO QDs@3DOM TiO_2.

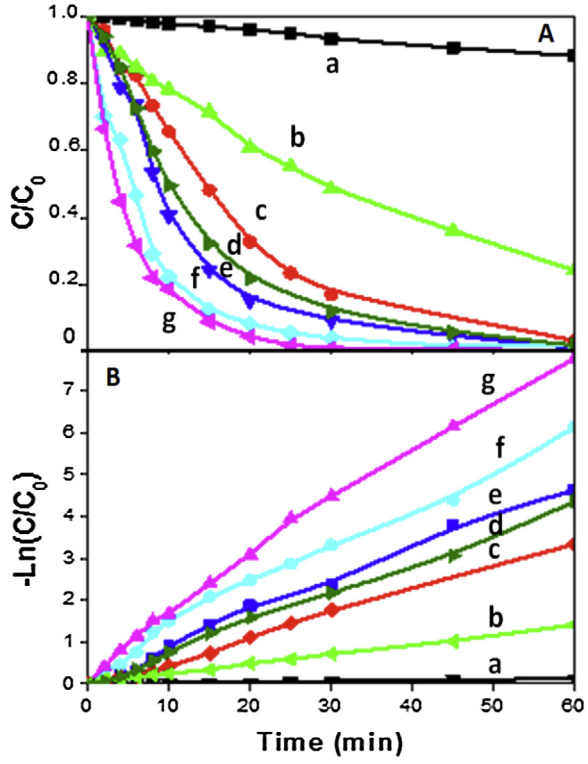

Fig. 11. (A) Evolution of RhB relative concentrations (C/C_0) with irradiation time for blank test (a) and different photocatalysts (b–f), (B) Kinetic curves of RhB photocatalytic degradation: (a) Blank, (b) P25, (c) 3DOM TiO_2, (d) 0.052 ZnO@3DOM TiO_2, (e) 0.026ZnO QDs@3DOM TiO_2, (f) 0.04ZnO QDs@3DOM TiO_2 and (g) 0.052ZnO QDs@3DOM TiO_2.

QDs@3DOM TiO_2 > 0.026ZnO QDs@3DOM TiO_2 > 0.052 ZnO@3DOM TiO_2 > 3DOM TiO_2 > P25. The results show clearly that, thanks to the introduction of ZnO QDs, the photocatalytic activity is tremendously improved compared with pure 3DOM TiO_2.

In order to quantify the reaction kinetics of RhB degradation in our experiments, the pseudo-first order model was employed using the linear transformation: $-\ln(C/C_0) = Kt$ (K is the kinetic constant). The results of this transformation are shown in Fig. 11B. The pseudo-first order reaction rate constants K extracted from linear fitting to curves in Fig. 11B for as-prepared 3DOM TiO_2, 0.026ZnO QDs@3DOM TiO_2, 0.04ZnO QDs@3DOM TiO_2 and

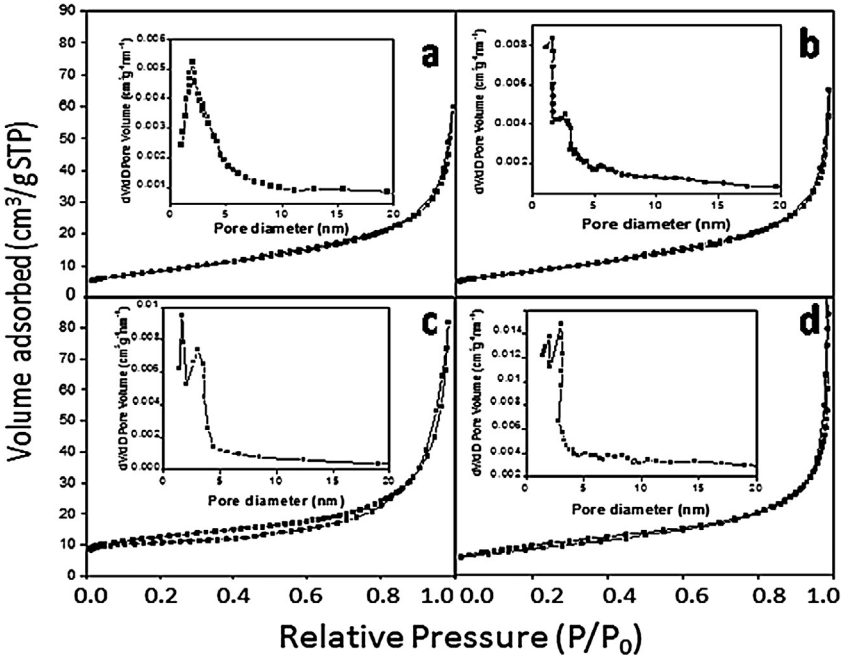

Fig. 10. Nitrogen adsorption–desorption isotherms and pore size distribution curves (insets) of the as-synthesized 3DOM TiO_2 (a), 0.026ZnO QDs@3DOM TiO_2 (b), 0.04ZnO QDs@ 3DOM TiO_2 (c), and 0.052ZnO QDs@3DOM TiO_2 (d).

0.052ZnO QDs@3DOM TiO_2 nanocomposites, are 0.062, 0.08, 0.098 and 0.129 min^{-1}, respectively. The Degussa P25 and the prepared 0.052 ZnO@3DOM TiO_2 nanocomposite were used as reference for comparison and their calculated kinetic constant were 0.0228 and 0.07 min^{-1}, respectively.

The photocatalytic activity of ZnO QDs@3DOM TiO_2 nanocomposite photocatalysts is strongly dependent on the amount of ZnO QDs. The 0.052ZnO QDs@3DOM TiO_2 nanocomposite has a photocatalytic activity 2 times higher than that of 3DOM TiO_2 and 5.5 times higher than that of P25, which demonstrates the high impact of the ZnO/TiO_2 heterojunction on the photocatalytic performance. The higher photocatalytic activity observed for 0.052 ZnO@3DOM TiO_2 than that of pure 3DOM TiO_2 confirms the role of ZnO-TiO_2 heterojunction. Indeed, as deduced from our PL and XPS studies, the formation of an intimate junction between ZnO QDs and TiO_2 increased the separation efficiency of the photogenerated electron-hole pairs by allowing interfacial charge transfer. On the other hand, the enhanced photocatalytic effect of the ZnO QDs@3DOM TiO_2 nanocomposites could be also generated by the 3DOM inverse opal structure, through the slow photon effect that enhanced light harvesting and therefore resulted in a higher photocatalytic activity. Moreover, besides heterojunction and slow light effects, the increased photocatalytic activity of nanocomposites based on nanostructured semiconductor can be stemmed from the quantum size effect. One consequence of the QSE is the increase of the band gap energy, which induces, in particular, a displacement of the conduction (valence) band towards the more negative (positive) region of the electrochemical scale of potentials allowing quick separation charge. The increase of the photogenerated charges energy and the ability of semiconductors to accumulate high densities of excess charge contribute to the photocatalytic process allowing the reduction of the e-h recombination in the volume of the semiconductor. In an electrochemical potential energy scale, the conduction band of TiO_2 is more positive than that of ZnO QDs, resulting in an inner electric field. As a result, the excited electrons can quickly transfer from ZnO QDs to TiO_2 conduction band and, consequently, the recombination of the photo-induced electron-hole pairs is greatly reduced. Besides, according to $\tau = \frac{r^2}{D\pi^2}$ [84] where τ is the average diffusion time from the bulk to the surface of the photogenerated carriers, r is the grain (or particle) radius and D is the diffusion coefficient of the carriers. As the particle size is reduced, the diffusion time is decreased resulting in an enhanced photocatalytic performance. From all the above, owing to the small size of ZnO QDs, the carriers can transfer to the photocatalyst surface rapidly and react with the reactants. Thus one important feature of QDs sensitized photocatalyst is the extremely short time τ_{diff} that is needed for diffusion of photogenerated charge carriers. Due to this short diffusion time, the reduction and oxidation reactions are more effective and takes place more quickly. For example, for 10 nm TiO_2 nanoparticles, the time for an electron to escape to the surface does not exceed 10 ps [85,86]. Robel et al. [87] studied size-dependent electron injection from excited CdSe QDs into TiO_2 nanoparticles and reported the tuning of the interparticle electron transfer rate by varying the QD particle size. They found that, as particle size decreases, the conduction band of CdSe QDs becomes more negative compared with that of TiO_2, which leads to enhanced electron transfer rate.

In our case the 0.052 ZnO QDs@3DOM TiO_2 exhibits an enhanced photocatalytic activity, about two times higher than that of 0.052 ZnO@3DOM TiO_2. This behavior can essentially be attributed to the QSE based on the discussion above.

It is well known that the efficiency of photocatalytic systems is conditioned by the separation of opposite charge carriers, suppressing the recombination processes which compete with charge transfer and thus reduce the quantum yield of the photocatalytic process. The ZnO QDs@3DOM TiO_2 heterojunction system is a good approach to achieve this charge separation.

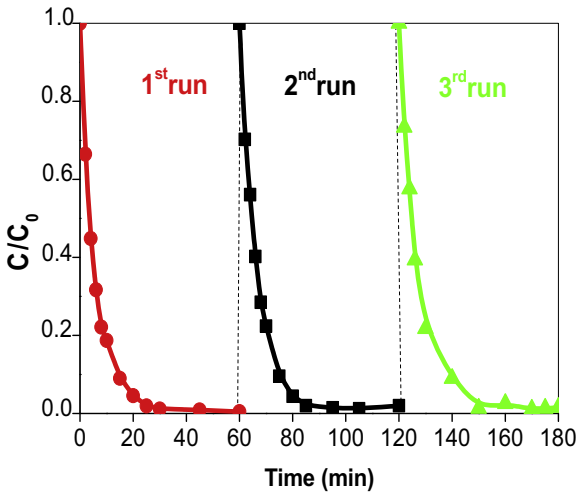

Fig. 12. Recycling runs in the photocatalytic degradation of Rhodamine B over the 0.052 ZnO QDs@3DOM TiO_2 photocatalyst.

Furthermore, to evaluate the durability and photocatalytic stability of the as-synthesized 0.052ZnO QDs@3DOM TiO_2 photocatalyst, the photocatalytic cycling tests were carried out under visible light irradiation, and each run lasted for 60 min (Fig. 12). It can be seen clearly that the 0.052ZnO QDs@3DOM TiO_2 nanocomposite does not exhibit any great loss in the activity after three times and the photodegradation performances are stable and the nanocomposite retain high photocatalytic ability in three successive runs each of which lasted for 60 min under visible-light irradiation, the RhB removal remained high at 98% in each of the three successive runs, which implied that the stability of ZnO QDs@3DOM TiO_2 is suitable for the photodegradation process of pollutants.

Due to the QSE band gap enlargement of ZnO QDs, the conduction band position of ZnO is displaced to more negative electrochemical potential energies. The CB and VB potentials of bulk ZnO was reported to be −0.42 V and 2.78 V versus normal hydrogen electrode (NHE), respectively [87]. However, for 5.5 nm ZnO QDs, the CB and VB potentials are −0.61 V and 2.86 V and the corresponding band gap energy is 3.48 eV [88]. For TiO_2, the CB and VB potentials are 2.91 V and −0.29 V, respectively, as reported in literatures [89–92]. Hence, the VB-CB energy difference between ZnO and TiO_2 is favorable for charge transfer. The energy band positions of bulk ZnO, ZnO QDs and TiO_2 are illustrated in Fig. 13.

Under UV irradiation both ZnO and TiO_2 are excited, the electrons of the VB of both ZnO QDs and TiO_2 are promoted to the CB, leaving holes behind. ZnO QDs, thanks to their more negative CB compared with TiO_2, are expected to have much stronger driving forces for injecting electrons from ZnO into TiO_2. The accumulated electrons in the conduction band of ZnO are prone to transfer to the CB of TiO_2. Electrons in the CB of TiO_2 are good reductants, which can capture the adsorbed O_2 and reduce it to O_2^- with subsequent transforming of water molecules into hydroxyl radicals for the oxidization of dye molecules. Concurrently, the photogenerated holes in the VB of TiO_2 diffused to the VB of ZnO. The holes at the VB of ZnO combined with H_2O to form hydroxyl radicals $OH^\bullet$. The so-formed active sites, $OH^\bullet$and O_2^-, could further degrade organic dye RhB into end products (H_2O and CO_2). In summary, this efficient charge separation increases lifetime of the charged carriers and enhances the efficiency of the interfacial-charged diffusion process and then enhanced the photocatalytic performance [93–95].

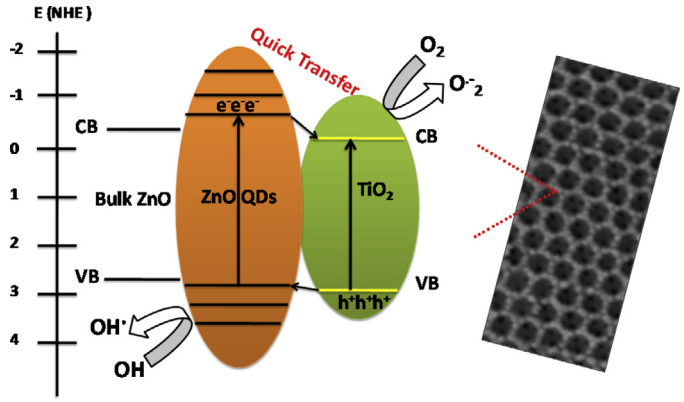

Fig. 13. Schematic representation of energy band diagram and charge transfer process in the ZnO QDs@3DOM TiO_2 nanocomposite under UV irradiation. Energy scale is defined with respect to normal hydrogen electrode (NHE).

4. Conclusions

We have synthesized a series of ZnO QDs@3DOM TiO_2 nanocomposites with intimate contact between both semiconductor components by the sol gel method combined with a polystyrene (PS) latex sphere templating technique. A highly enhanced photocatalytic performance is observed and explained by the synergetic effect involving a quantum size effect which results in the accumulation of high densities of excess charge with higher energies, and a structural effect in which 3DOM structures with an open interconnected porous network facilitate the diffusion of molecules and offer a larger surface area. In addition, the formation of ZnO/TiO_2 nanoheterojunctions, being quite favorable for photocatalysis and quick interfacial charge transfer, may lead to even higher quantum efficiency, supplying more photogenerated electrons in photocatalytic reactions. The present work is a successful example of the enhancement of photocatalytic activity by the combination of ZnO QDs and 3DOM semiconductor photocatalyst.

Acknowledgements

This work was realized with the financial support of the Belgian FNRS (Fonds National de la Recherche Scientifique) and by Chinese Ministry of Education in a framework of the Changjiang Scholar Innovative Research Team Program (IRT_15R52). B.L. Su acknowledges the Chinese Central Government for an "Expert of the State" position in the Program of the "Thousand Talents" and a Clare Hall Life Member, University of Cambridge. Y. Li acknowledges Hubei Provincial Department of Education for the "Chutian Scholar" program. This work is also supported by PhD Programs Foundation (20120143120019) of Chinese Ministry of Education, the Wuhan Youth Chenguang Program of Science and Technology (2013070104010003), Hubei Provincial Natural Science Foundation (2014CFB160, 2015CFB516), the National Science Foundation for Young Scholars of China (No. 51502225) and Self-determined and Innovative Research Funds of the SKLWUT (2015-ZD-7). This research used resources of the Electron Microscopy Service located at the University of Namur. This Service is member of the "Plateforme Technologique Morphologie – Imagerie". The XPS analyses were made in the LISE, Department of Physics of University of Namur thanks to Dr. P. Louette. XRD measurements, UV–vis and photoluminescent spectroscopic analyses and N_2 adsorption-desorption measurements were made with the facility of the "Plateforme Technologique Physico-Chimique".

References

[1] Q.H. Zhang, L. Gao, J.K. Guo, Appl. Catal. B 26 (2000) 207–215.
[2] R.Y. Hong, J.H. Li, L.L. Chen, D.Q. Liu, H.Z. Li, Y. Zheng, J. Ding, Powder Technol. 189 (2009) 426–432.
[3] Y.N. Huo, Y. Jin, J. Zhu, H.X. Li, Appl. Catal. B 89 (2009) 543–550.
[4] R.D. Gould, A.K. Hassan, F.S. Mahmoid, Int. J. Electron. 76 (1994) 895.
[5] G.B. Zhang, C.S. Shi, Z.F. Han, J.Y. Shi, Z.X. Fu, M. Kirm, G. Zimmerer, Chin. Phys. Lett. 18 (2001) 441–442.
[6] M.R. Hoffmann, S.T. Martin, W.Y. Choi, D.W. Bahnemann, Chem. Rev. 95 (1995) 69–96.
[7] M. Zhou, J. Zhang, B. Cheng, H. Yu, Int. J. Photoenergy 10 (2012) 532843.
[8] H. Choi, E. Stathatos, D.D. Dionysiou, Appl. Catal. B 63 (2006) 60–67.
[9] K. Lv, J. Yu, K. Deng, X. Li, M. Li, J. Phys. Chem. Solids 71 (2010) 519–522.
[10] H. Li, Z. Bian, J. Zhu, Y. Huo, H. Li, Y. Lu, J. Am. Chem. Soc. 129 (2007) 4538–4539.
[11] V. Iliev, D. Tomova, R. Todorovska, Appl. Catal. A 313 (2006) 115–121.
[12] R. Bacsa, J. Kiwi, T. Ohno, P. Albers, V. Nadtochenko, J. Phys. Chem. B 109 (2005) 5994–6003.
[13] J.A. Rengifo-Herrera, C. Pulgarin, Sol. Energy 84 (2010) 37–43.
[14] D.S. Bhatkhande, V.G. Pangarkar, A. Beenackers, J. Chem. Technol. Biotechnol. 77 (2002) 102–116.
[15] M.A. Hasnat, M.M. Uddin, A.J.F. Samed, S.S. Alam, S. Hossain, J. Hazard. Mater. 147 (2007) 471–477.
[16] A. Akyol, M. Bayramoglu, J. Hazard. Mater. 175 (2010) 484–491.
[17] G. Marcì, V. Augugliaro, M.J. López-Munoz, C. Martín, L. Palmisano, V. Rives, J Phys. Chem. B 105 (2001) 1033–1040.
[18] D. Chen, H. Zhang, S. Hu, J.H. Li, J. Phys. Chem. C 112 (2008) 117–122.
[19] M. Law, L.E. Greene, A. Radenovic, T. Kuykendall, J. Liphardt, P.D. Yang, J. Phys. Chem. B 110 (2006) 22652–22663.
[20] L.E. Greene, M. Law, B.D. Yuhas, P.D. Yang, J. Phys. Chem. C 111 (2007) 18451–18456.
[21] R.S. Mane, W.J. Lee, H.M. Pathan, S.H. Han, J. Phys. Chem. B 109 (2005) 24254–24259.
[22] S.W. Ding, L.Y. Wang, S.Y. Zhang, S.J. Liu, Y. Ding, Y.C. Liu, Chin. J. Inorg. Chem. 19 (2003) 631.
[23] H.B. Jiang, L. Gao, Q.H. Zhang, J. Inorg. Mater. 18 (2003) 695–698.
[24] N. Serpone, P. Maruthamuthu, P. Pichat, E. Pelizzetti, H.J. Hidaka, J. Photochem. Photobiol. A: Chem. 85 (1995) 247–255.
[25] O. Carp, C.L. Huisman, A. Reller, Prog. Solid State Chem. 32 (2004) 33–177.
[26] Q. Wang, C.C. Chen, D. Zhao, W.H. Ma, J.C. Zhao, Langmuir 24 (2008) 7338.
[27] F. Chen, J.C. Zhao, H. Hidaka, Int. J. Photoenergy 5 (2003) 209.
[28] X.F. Hu, T. Mohamood, W.H. Ma, C.C. Chen, J.C. Zhao, J. Phys. Chem. B 110 (2006) 26012.
[29] S.K. Kansal, M. Singh, D. Sud, J. Hazard. Mater. 141 (2007) 581–590.
[30] K. Yu, S. Yang, H. He, C. Sun, C. Gu, Y. Ju, J. Phys. Chem. A 113 (2009) 10024–10032.
[31] M. Sun, D. Li, Y. Chen, W. Chen, W. Li, Y. He, X. Fu, J. Phys. Chem. C 113 (2009) 13825–13831.
[32] Z. He, C. Sun, S. Yang, Y. Ding, H. He, Z. Wang, J. Hazard. Mater. 162 (2009) 1477–1486.
[33] J. Luan, M. Li, K. Ma, Y. Li, Z. Zou, Chem. Eng. J. 167 (2011) 162–171.
[34] A. Mehrdad, B. Massoumi, R. Hashemzadeh, Chem. Eng. J. 168 (2011) 1073–1078.
[35] W. Sun, Y. Yu, H. Pan, X. Gao, Q. Chen, L. Peng, J. Am. Chem. Soc. 130 (2008) 1124–1125.
[36] D. Liu, Z. Zheng, C. Wang, Y. Yin, S. Liu, B. Yang, Z. Jiang, J. Phys. Chem. C 117 (2013) 26529–26537.
[37] I. Dube, V. Fabian Ruiz-Ruiz, D. Diaz, S. Posadas, A. Zeinert, J. Phys. Chem. C 118 (2014) 11495–11504.
[38] W. Ho, J.C. Yu, J. Lin, J. Yu, P. Li, Langmuir 20 (2004) 5865–5869.
[39] J. Yu, Y. Hai, M. Jaroniec, J. Colloid Interface Sci. 357 (2011) 223–228.
[40] J. Yu, J. Zhang, M. Jaroniec, Green Chem. 12 (2010) 1611–1614.
[41] F.A. Frame, F.E. Osterloh, J. Phys. Chem. C 114 (2010) 10628–10633.
[42] M.A. Holmes, T.K. Townsend, F.E. Osterloh, Chem. Commun. 48 (2012) 371–373.
[43] C. Wang, R.L. Thompson, P. Ohodnicki, J. Baltrus, C. Matranga, J. Mater. Chem. 21 (2011) 13452–13457.
[44] G. Ramakrishna, H.N. Ghosh, Langmuir 19 (2003) 3006–3012.
[45] L. Spanhel, H. Weller, A. Henglein, J. Am. Chem. Soc. 109 (1987) 6632–6635.
[46] K. Huang, L. Chen, J. Deng, J. Xiong, J. Nanomater. 12 (2012) 720491.
[47] W. Ho, J.C. Yu, J. Mol. Catal. A 247 (2006) 268–274.
[48] W. Ho, J.C. Yu, J. Lin, P. Li, Langmuir 20 (2004) 5865–5869.
[49] Y. Xie, G. Ali, S. Hwa Yoo, S. Oh Cho, Appl. Mater. Interfaces 10 (2010) 2910–2914.
[50] P. Wang, D. Li, J. Chen, X. Zhang, J. Xian, X. Yang, X. Zheng, X. Li, Y. Shao, Appl. Catal. B 160-161 (2014) 217–226.
[51] A. Stein, F. Li, N.R. Denny, Chem. Mater. 20 (2008) 649–666.
[52] H. Zhao, M. Wu, J. Liu, Z. Deng, Y. Li, B.L. Su, Appl. Catal. B 184 (2016) 182–190.
[53] (a) M. Wu, A. Zheng, F. Deng, B.L. Su, Appl. Catal. B 138-139 (2013) 219–228;
(b) M. Wu, J. Jin, J. Liu, Z. Deng, Y. Li, O. Deparis, B.L. Su, J. Mater. Chem. A 1 (2013) 15491–15500;
(c) J. Liu, J. Jin, Y. Li, H.W. Huang, C. Wang, M. Wu, L.H. Chen, B.L. Su, J. Mater. Chem. A 2 (2014) 5051–5059;
(d) M. Wu, J. Liu, J. Jin, C. Wang, S.Z. Huang, Z. Deng, Y. Li, B.L. Su, Appl. Catal. B

150–151 (2014) 411–420;
(e) M. Wu, Y. Li, Z. Deng, B.L. Su, ChemSusChem 4 (2011) 1481–1488.
[54] X. Zheng, D. Li, X. Li, J. Chen, C. Cao, J. Fang, J. Wang, Y. He, Y. Zheng, Appl. Catal. B 168–169 (2015) 408.
[55] L. Li, Y.H. Zhao, L.E. Shuai, N. Zhuo, H.Y. Ma, B. Liu, Chem. J. Chin. Uiver. 32 (2011) 1323–1329.
[56] J. Liu, M. Li, J. Wang, Y. Song, L. Jiang, T. Murakami, A. Fujishima, Environ. Sci. Technol. 43 (2009) 9425–9431.
[57] J.I.L. Chen, E. Loso, N. Ebrahim, G.A. Ozin, J. Am. Chem. Soc. 130 (2008) 5420–5421.
[58] O. Deparis, S.R. Mouchet, B.L. Su, Phys. Chem. Chem. Phys. 17 (2015) 30525–30532.
[59] Y. Wang, H. Dai, J. Deng, Y. Liu, H. Arandiyan, X. Li, B. Gao, S. Xie, Solid State Sci. 24 (2013) 62–70.
[60] T. Wang, X. Yan, S. Zhao, B. Lin, C. Xue, G. Yang, S. Ding, B. Yang, C. Ma, G. Yang, G. Yang, J. Mater. Chem. A 2 (2014) 15611–15619.
[61] K. Ji, H. Dai, J. Deng, H. Zang, H. Arandiyan, S. Xie, H. Yang, Appl. Catal. B 168 (2015) 274–282.
[62] K. Ji, J. Deng, H. Zang, J. Han, H. Arandiyan, H. Dai, Appl. Catal. B 165 (2015) 285–295.
[63] M. Zalfani, B. Van Der Schueren, Z.Y. Hu, J. Rooke, R. Bourguiga, M. Wu, G. Van Tendeloo, Y. Li, B.L. Su, J. Mater. Chem. A 3 (2015) 21244–21256.
[64] J. Jiao, Y. Wei, Z. Zhao, J. Liu, J. Li, A. Duan, G. Jiang, Ind. Eng. Chem. Res. 53 (2014) 17345–17354.
[65] M.K. Patra, M. Manoth, V.K. Singh, G. SiddaramanaGowd, V.S. Choudhry, S.R. Vadera, N. Kumar, J. Lumin. 129 (2009) 320–324.
[66] Y. Wan, S. Wang, W. Luo, L. Zhao, Int. Photoenergy 2012 (2012) 392865.
[67] Z.Y. Yuan, T.Z. Ren, A. Vantomme, B.L. Su, Chem. Mater. 16 (2004) 5096–5106.
[68] M. Futsuhara, K. Yoshioka, O. Takai, Thin Solid Films 322 (1998) 274–281.
[69] X. Xue, W. Ji, Z. Mao, H. Mao, Y. Wang, X. Wang, W. Ruan, B. Zhao, J.R. Lombardi, J. Phys. Chem. C 116 (2012) 8792–8797.
[70] L.Q. Jing, X.J. Sun, B.F. Xin, B.Q. Wang, W.M. Cai, H.G. Fu, J. Solid State Chem. 177 (2004) 3375–3382.
[71] J. Cao, B. Luo, H. Lin, B. Xu, S. Chen, Appl. Catal. B111-112 (2012) 288–296.
[72] J. Cao, B. Luo, H. Lin, B. Xu, S. Chen, Appl. Catal. B: Environ. 111 (2012) 288.
[73] J.M. Herrmann, H. Tahiri, Y. Ait-Ichou, G. Lassaletta, A.R. Gonzalez-Elipe, A. Fernandez, Appl. Catal. B 13 (1997) 219.
[74] J. Li, L. Liu, Y. Yu, Y. Tang, H. Li, F. Du, Electrochem. Commun. 6 (2004) 940.
[75] Y. Ma, X.L. Wang, Y.S. Jia, X.B. Chen, H.X. Han, C. Li, Chem. Rev. 114 (2014) 9987–10043.
[76] W.F. Zhang, M.S. Zhang, Z. Yin, Q. Chen, Appl. Phys. B: Lasers Opt. 70 (2000) 261–265.
[77] L.Q. Jing, X.J. Sun, B.F. Xin, B.Q. Wang, W.M. Cai, H.G. Fu, J. Solid State Chem. 177 (2004) 3375–3382.
[78] J. Cao, B. Luo, H. Lin, B. Xu, S. Chen, Appl. Catal. B 111–112 (2012) 288–296.
[79] S.K. Mohanta, S.H. Lee, B.H. Kong, H.K. Cho, J. Cryst. Growth 311 (2009) 1539–1544.
[80] R. Georgekutty, M.K. Seery, S.C. Pillai, J. Phys. Chem. C 112 (2008) 13563–13570.
[81] Q.C. Xu, D.V. Wellia, Y.H. Ng, R. Amal, T.T.Y. Tan, J. Phys. Chem. C 115 (2011) 7419–7428.
[82] X. Liu, Z. Liu, J. Zheng, J. Alloy. Compd. 509 (2011) 9970–9976.
[83] S.J. Gregg, K.S.W. Sing, Adsorption Surface Area and Porosity, 2nd edition, Academic Press, London, UK, 1982.
[84] W.C. Li, A.H. Lu, C. Weidenthaler, F. Schüth, Chem. Mater. 16 (2004) 5676–5681.
[85] A. Hagfeldt, M. Grätzel, Chem. Rev. 95 (1995) 49–68.
[86] K. Jortner, C. Rao, Pure Appl. Chem. 74 (2002) 1491–1506.
[87] I. Robel, M. Kuno, P.V. Kamat, J. Am. Chem. Soc. 129 (2007) 4136–4137.
[88] J. Jacobsson, T. Edvinsson, J. Phys. Chem. C116 (2012) 15692–15701.
[89] A.L. Stroyuk, A.I. Kryukov, S.Y. Kuchmii, V.D. Pokhodenko, Theo. Exp. Chem. 41 (2005) 207–228.
[90] Q. Teng, X. Zhou, B. Jin, J. Luo, X. Xu, H. Guan, W. Wang, F. Yang, RSC Adv. 6 (2016) 36881–36887.
[91] D. Zhang, X. Li, H. Tan, G. Zhang, Z. Zhao, H. Shi, L. Zhang, W. Yu, Z. Sun, RSC Adv. 4 (2014) 44322–44326.
[92] X. Zhong, M. Jin, H. Dong, L. Liu, L. Wang, H. Yu, S. Leng, G. Zhuang, X. Li, J.G. Wang, J. Solid State Chem. 220 (2014) 54–59.
[93] T. Inoue, A. Fujishima, S. Konishi, K. Honda, Nature 277 (1979) 637.
[94] W.C. Li, A.H. Lu, C. Weidenthaler, F. Schüth, Chem. Mater. 16 (2004) 5676–5681.
[95] D.L. Liao, C.A. Badour, B.Q. Liao, J. Photochem. Photobiol. A 194 (2008) 11–19.